Tectonophysics 617 (2014) 114–125

Contents lists available at ScienceDirect

Tectonophysics

journal homepage: www.elsevier.com/locate/tecto

Short- and long-term earthquake triggering along the strike-slip Kunlun fault, China: Insights gained from the M_s 8.1 Kunlun earthquake and other modern large earthquakes

Chaodi Xie [a,*], Xinglin Lei [b], Xiaoping Wu [a], Xionglin Hu [c]

[a] Department of Geophysics, Yunnan University, Kunming 650091, China
[b] Geological Survey of Japan, National Institute of Advanced Industrial Science and Technology, Tsukuba 305-8567, Japan
[c] Earthquake Administration of Yunnan Province, Kunming 650041, China

ARTICLE INFO

Article history:
Received 21 August 2012
Received in revised form 14 January 2014
Accepted 19 January 2014
Available online 24 January 2014

Keywords:
Coulomb failure stress change
Viscous relaxation
ETAS model
Kunlun fault
Short-and long-term seismic triggering

ABSTRACT

Following the 2001 M_s8.1 Kunlun earthquake, earthquake records of more than 10 years, in addition to more than one century's records of large earthquakes, provide us with a chance to examine short-term (days to a few years) and long-term (years to decades) seismic triggering following a magnitude ~8 continental earthquake along a very long strike-slip fault, the Kunlun fault system, located in northern Tibet, China. Based on the calculations of coseismic Coulomb stress changes (ΔCFS) from the larger earthquake and post-seismic stress changes due to viscoelastic stress relaxation in the lower crust and upper mantle, we examined the temporal evolution of seismic triggering. The ETAS (epidemic type aftershocks sequence) model shows that the seismic rate in the aftershock area over ~10 years was higher than the background seismicity before the mainshock. Moreover, we discuss long-term (years to decades) triggering and the evolution of stress changes for the sequence of five large earthquakes of M ≥7.0 that ruptured the Kunlun fault system since 1937. All subsequent events of M ≥7.0 occurred in the regions of positive accumulated ΔCFS. These results show that short-term (up to 200 days in our case) triggering along the strike-slip Kunlun fault is governed by coseismic stress changes, while long-term triggering is somewhat due to post-seismic Coulomb stress changes resulting from viscoelastic relaxation.

1. Introduction

There is increasing evidence that the redistribution of stress induced by large earthquakes can lead to changes in seismicity or even trigger large earthquakes (Gomberg et al., 1998; Harris, 1998; Kilb et al., 2002; King et al., 1994; Reasenberg and Simpson, 1992). These studies assert that stress changes may affect the properties of nearby faults and advance fault rupture, finally triggering impending earthquakes; these mechanisms may be divided into static stress triggering and dynamic stress triggering. The former focuses on the triggering effects of static stress changes due to fault dislocation (Anderson and Johnson, 1999; Caskey and Wesnousky, 1997; King et al., 1994; Toda et al., 2008); the latter focuses on the triggering effects of transient or dynamic stress changes due to the passing of seismic waves (Brodsky et al., 2000; Gomberg et al., 1998; Lei et al., 2011). Generally, both dynamic and static triggering use Coulomb failure stress changes (ΔCFS) to explain the triggering of earthquakes (Anderson and Johnson, 1999; Caskey and Wesnousky, 1997; Catalli et al., 2008; Felzer et al., 2002; Marsan, 2003; Pollitz and Sacks, 2002; Reasenberg and Simpson, 1992; Stein, 1999; Stein et al., 1994, 1997; Toda and Stein, 2003; Toda et al., 2008).

In most cases, the seismic triggering of large events happens in days to months, such as the Big Bear earthquake, which occurred only 3 h after the Landers earthquake (King et al., 1994) (which we have termed as "short-term triggering"). However, large earthquakes can trigger events over years to tens of years (which we have termed as "long-term triggering"), such as the 1999 M_w 7.1 Hector Mine earthquake which is thought to be triggered seven years after the Landers earthquake (Pollitz and Sacks, 2002; Zeng, 2001). Recent studies (Lorenzo-Martin et al., 2006; Pollitz and Sacks, 2002; Zeng, 2001) have suggested that a relationship exists between long-term triggering processes and post-seismic stress changes from viscous relaxation in the lower crust and upper mantle.

To date, there have been many studies of short-term triggering (Brodsky et al., 2000; Caskey and Wesnousky, 1997; Husen et al., 2004; Husker and Brodsky, 2004; Kilb et al., 2002; Marsan, 2003; Moran et al., 2004; Stein et al., 1992; Toda et al., 2008) because it is easier to demonstrate a direct correlation between triggered seismicity and the distribution of coseismic ΔCFS that is transferred from the mainshock. However, long-term seismic triggering needs more

* Corresponding author. Tel.: +86 15198972728.
E-mail address: xiecd@ynu.edu.cn (C. Xie).

0040-1951/$ – see front matter © 2014 Elsevier B.V. All rights reserved.
http://dx.doi.org/10.1016/j.tecto.2014.01.023

attention. Moreover, it is well documented that large earthquakes trigger their own aftershocks, with a decreasing event rate following the modified Omori's law (Brodsky et al., 2000; Felzer et al., 2002; Helmstetter and Sornette, 2003a; Husen et al., 2004). However, triggering of large earthquakes following a large mainshock still remains poorly understood.

The M_s 8.1 (M_w 7.8) Kunlun earthquake on 14 November 2001 ruptured more than 400 km of the western part of the Kunlun fault in the northern Tibetan Plateau, with a maximum horizontal slip ranging between 7.5 and 10 m (Lasserre et al., 2005; Van der Woerd et al., 2003; Xu et al., 2002). It was one of the largest continental strike-slip earthquakes recorded by modern seismic instruments to date. Immediately after the mainshock, the regional seismic network recorded a large number of local earthquakes throughout the Kunlun region, including more than 20 events of $M \geq 3.7$ occurring within the 1st 24 h and 5 events of $M \geq 5.0$ occurring within the first month. Moreover, the apparent increase in regional seismicity continued for approximately ten years after the mainshock. The clustering of seismic activity may imply that most earthquakes are early aftershocks of the Kunlun earthquake (Van der Woerd et al., 2002). We are interested in verifying the correlation between the aftershock distribution of subsequent earthquake sequences and the stress changes caused by the mainshock. One goal of this paper is to carefully examine the statistical significance of the seismic rate increase and the detailed features of seismic triggering. The 10-year postseismic catalogue of earthquakes and the number of modern large earthquakes in this region afford an opportunity to address both short- and long-term triggering issues after magnitude 7–8 strike-slip earthquakes, which is the most significant aspect of this study.

In this work, we calculated both the coseismic stress change and the post-seismic stress changes due to viscoelastic relaxation in order to investigate short- and long-term seismic triggering processes. Our study begins with the calculations of Coulomb stress changes. We then perform statistical analyses of the subsequent seismicity to detect significant anomalies in seismicity that are associated with static stress changes. Finally, we discuss long-term triggering associated with the large earthquake sequence of $M \geq 7.0$ along the Kunlun fault system.

2. Seismological and tectonic setting

The U.S. Geological Survey (USGS) determined that the epicentre of the 14 November 2001 M_s 8.1 Kunlun earthquake was 35.95°N and 90.54°E, located in the Kokoxili region of the northwest part of Qinghai province. This event is thus also called the Kokoxili earthquake. It produced a long surface rupture zone with a length of 350–400 km along the Kunlun fault in northern Tibet (Fig. 1) (Fu et al., 2005, and references herein). Together with the Altyn Tagh fault, the Haiyuan fault, the Xianshui He fault, and the Karakorum fault, the Kunlun fault is one of the main faults accommodating both the northeastward shortening and the eastward extrusion of the Tibet plateau in response to the ongoing collision between Asia and India (Klinger et al., 2005; Tapponnier and Molnar, 1977; Tapponnier et al., 2001). All of these are left-lateral strike-slip fault systems, except for the Karakorum fault, which is a right-lateral strike-slip fault (Fig. 1) (Molnar and Lyon-Caen, 1989). From cosmogenic dating of offset alluvial terraces along the fault, the long-term slip rate along much of the Kunlun fault has been determined to be 11.5 ± 2.0 mm/year, over a time span of ~40,000 years (Van der Woerd et al., 2000, 2001, 2002). The Kunlun fault is not only one of the faults associated with the extrusion of the Tibetan plateau but is also an example of a large-scale strike-slip fault system in the continental crust (Van der Woerd et al., 2002).

The Kunlun fault system, including the Manyi fault at its west, has a total length of approximately 1600 km, extending from 86°E to 105°E, with an average strike of N100°E. Based on the geometry of the fault trace, the main stretch of the Kunlun fault may be divided into six principal segments (Van der Woerd et al., 2001). Several large ($M > 7$) earthquakes have ruptured different segments in the last 100 years (Fig. 1). The 2001 earthquake ruptured the westernmost, or Kusai Hu segment, named for the large lake it crosses (Fig. 1). This 270-km segment is geologically the clearest segment of the Kunlun fault. It is remarkably straight between 91°E and 94°E and shows a progressive change in strike, from N100°E in the west to N95°E in the east. Such a specific geometry causes slightly different styles of faulting, from oblique normal-strike-slip, to nearly pure strike-slip and oblique reverse-strike-slip faulting (Van der Woerd et al., 2001). Prior to 2001,

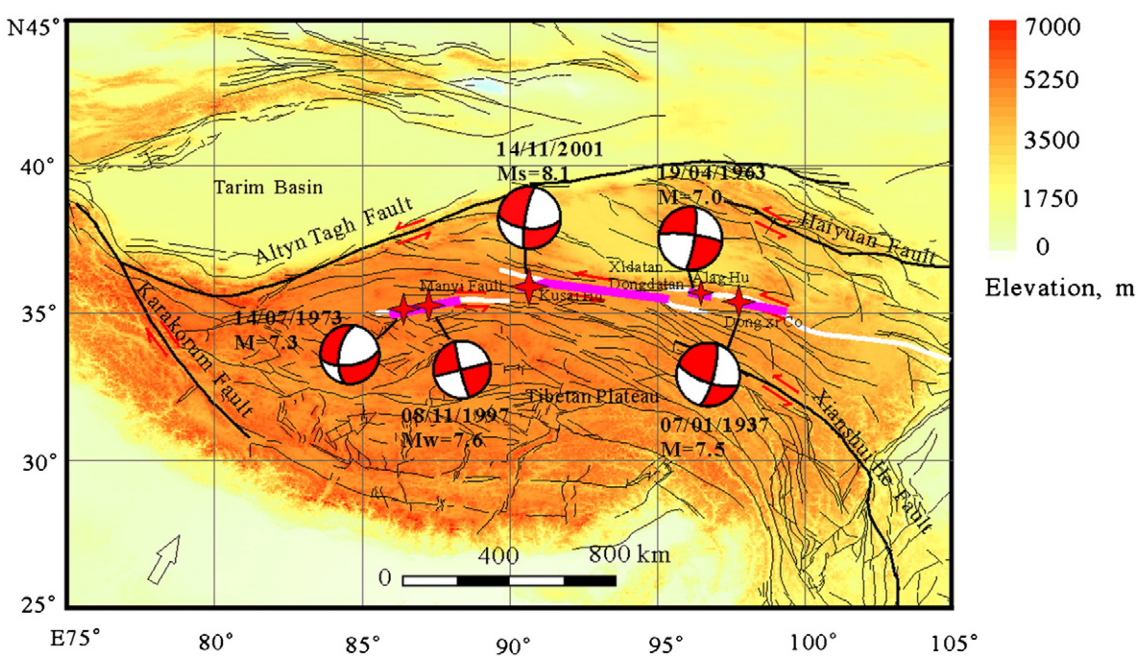

Fig. 1. Map of the Tibetan plateau and adjacent regions of the Kunlun fault. The thick white lines indicate the Kunlun fault system, and the thick pink lines represent segments ruptured by large modern earthquakes. Grey and black lines show traces of faults. Stars indicate the locations of large events along the Kunlun fault: the 1937 M 7.5 DongXi Co earthquake, the 1963 M 7.0 Dulan earthquake, the 1973 M 7.3 Manyi earthquake, the 1997 M_w 7.6 Manyi earthquake, and the 2001 M_s 8.1 Kunlun earthquake. Corresponding focal mechanisms are from Molnar and Deng (1984) and the Harvard CMT solution.

no large earthquake of M ≥7.0 had been instrumentally recorded along the Kusai Hu segment. To the west, the 1997 M_w 7.6 earthquake produced a 170-km surface rupture along the Manyi fault, which is considered to be a branch fault of the Kunlun fault system (Lin et al., 2006; Xu, 2000). Farther west, a magnitude ~7.3 earthquake occurred in 1973 at the western end of the Manyi segment (Fig. 1). Since 1930, two large historic events have occurred along the two eastern segments of the Kunlun fault. The 1937 M ~7.5 earthquake ruptured most of the Dongxi Co segment (Fig. 1), resulting in a 150-km length of surface rupture (Van der Woerd et al., 2000, 2001). In 1963, another earthquake of magnitude ~7.0 occurred approximately 100 km west of the 1937 event epicentre, along the Alag Hu segment (Fig. 1) (Van der Woerd et al., 2001). The focal mechanisms of these historic earthquakes show a distinct left-lateral strike-slip motion (Gu et al., 1989; Molnar and Deng, 1984). It is worth noting that no large events have been recorded so far on the Xidatan–Dongdatan segment, which is between the Kusai Hu segment and Alag Hu segment.

3. Seismicity following the M_s 8.1 Kunlun earthquake

Here we focus on the seismic activity associated with the 2001 M_s 8.1 Kunlun earthquake. Thus, the study area is bounded by a rectangle with coordinates 35°–37°N and 89°–98°E, which is along the rupture plane of the mainshock. The seismic catalogue for this area is obtained from the China Earthquake Data Centre, and M_L magnitudes are given for all events. The minimum magnitude of completeness (M_c), above which all earthquakes are detected by the seismic network, is estimated by calculating the magnitude–frequency distributions for earthquakes that occurred in two time spans: 2001 through 2011 and 1990 through 2011 (Fig. 2a–b). The scatter plot of magnitude against the sequential number of events indicates the lower cut-off magnitudes used in this study (Fig. 2c). However, the catalogue also contains many events with a magnitude of less than M_c. Seismic activity is usually studied using data of magnitude $\geq M_c$. However, earthquakes $<M_c$, which are usually substantial, may also contribute to the study of the spatial association. Therefore, when we examined the statistical correlation between aftershocks and the Coulomb stress changes, we also used events having a magnitude under the lower cut-off value for M_c in our analyses.

Figs. 3–4 display the seismicity following the M_s 8.1 Kunlun earthquake in the study area. More than 20 aftershocks occurred within the 1st 24 h after the Kunlun earthquake. In the first year after the mainshock, a large number of events occurred, primarily at sites adjacent to the eastern segment of the ruptured fault, including some events of M ≥5.0. In the next several years after the mainshock, earthquakes clustered close to the western segment of the ruptured fault. Fig. 3a also shows focal mechanisms from the Harvard CMT solution for some M ≥5.0 events. Most events following the Kunlun earthquake have had shallower focal depths (≤40 km). Only a few events had deeper focal depths (up to 80 km), which may be caused by location error (Fig. 3b). It is interesting to note that the largest aftershock of the M_s 8.1 Kunlun earthquake had a magnitude of 5.6, significantly smaller than the size predicted (~6.5) by Båth's law (Helmstetter and Sornette, 2003b).

Fig. 4 shows cumulative numbers of the seismicity in the study area with various cut-off magnitudes, demonstrating a typical pattern of aftershock activity. It is worth noting that no M5+ events have occurred since 2007. After 2010, the seismic rate of both M3+ and M4+ events is clearly lower than the background seismicity before the Kunlun earthquake. This is probably a sign of the end of the aftershock phase, but further data are needed before a conclusive assessment can be reached.

4. Analysis of seismic triggering following the M_s 8.1 Kunlun earthquake

To investigate the spatial correlation of seismicity and stress changes, we calculated the static Coulomb failure stress change that was imparted by the 2001 Kunlun earthquake. The static Coulomb failure stress change is expressed as $\Delta CFS = \Delta\tau + \mu'\Delta\sigma$, where $\Delta\sigma$, and $\Delta\tau$ are changes in the normal stress (positive when unclamped) and the shear stress, respectively, calculated on a given receiver fault and given slip direction, and μ' is the effective coefficient of friction (Harris, 1998; King et al., 1994; Toda and Stein, 2002, 2003). Based on the Mohr–Coulomb failure criterion, a positive Coulomb failure stress change is expected to promote failure and a negative value to inhibit failure.

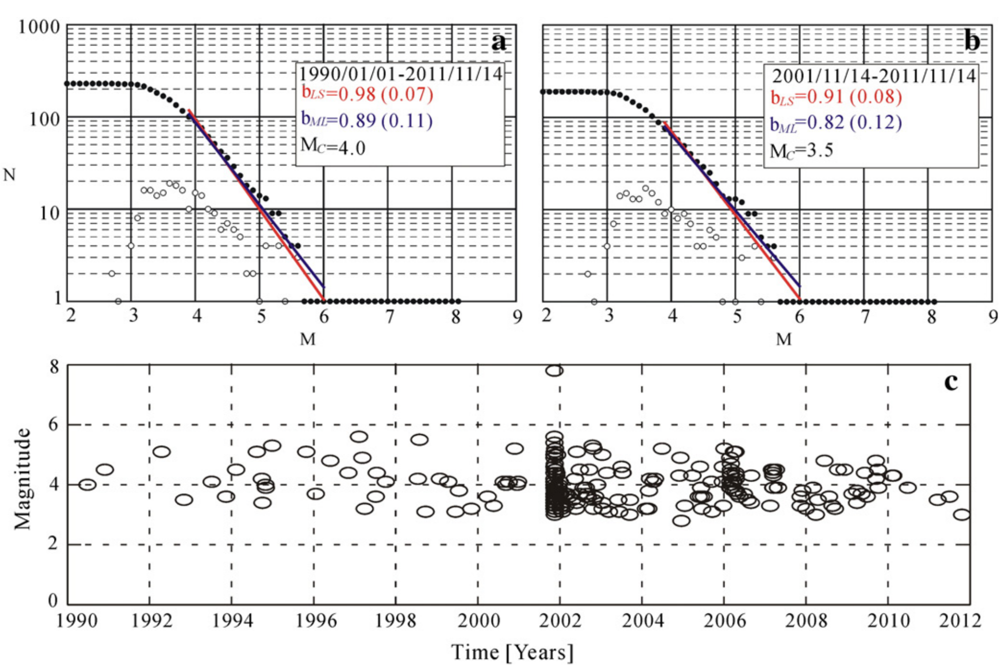

Fig. 2. Cumulative magnitude–frequency distributions for earthquakes in the study area (a, b). M_c indicates the minimum magnitude of completeness. The maximum likelihood *b* values and the least square *b* values are shown by b_{ML} and b_{LS}, respectively. Numbers in parentheses indicate the standard errors. The scatter plot of magnitude against sequential number of events indicates the lower cut-off magnitudes used in this study (c).

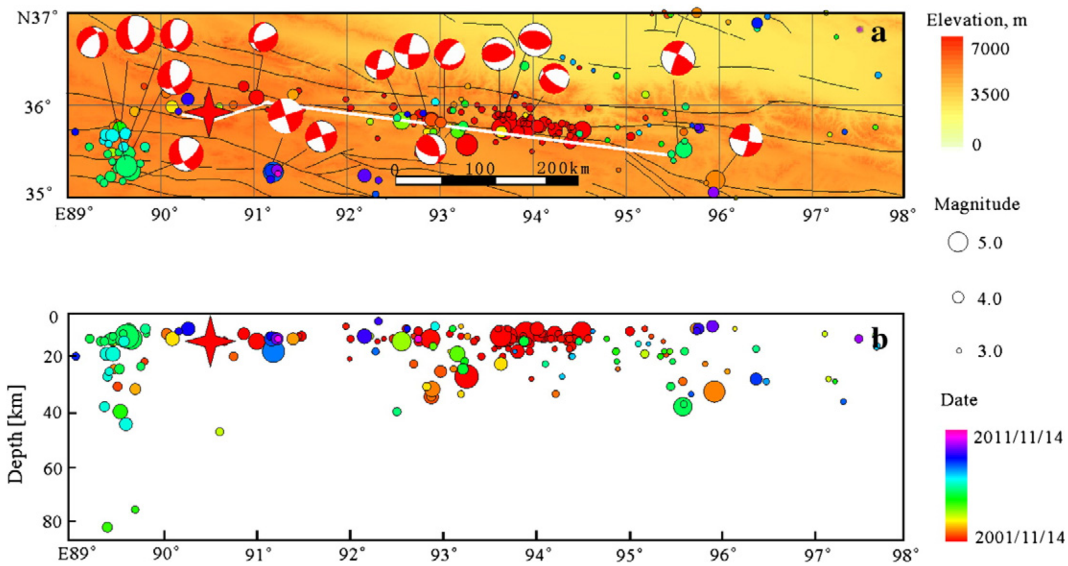

Fig. 3. Seismicity for a period between the 2001 Kunlun earthquake and 14 November 2011. The coloured circles represent earthquake epicentres as established by the China Earthquake Data Centre. The hypocentre locations are colour coded by time and scaled by magnitude as indicated. The white lines show the projection of the (nearly vertical) rupture plane of the 2001 Kunlun earthquake on the surface (from Wen et al., 2009). The red star marks the 2001 Kunlun mainshock. The red beach ball indicates the focal mechanism from the Harvard CMT solution of the M >5.0 event. In (b), the depth section of event hypocentres is plotted.

Here we first compute the static ΔCFS due to the coseismic rupture in an elastic half-space (Okada, 1992) with a friction coefficient $\mu' = 0.6$ and a Poisson's ratio of 0.25. The shear modulus is assumed to be 3.2×10^{10} Nm^{-2}. Furthermore, to explore long-term earthquake triggering, we used a more realistic lithologic model in which the upper mantle and the lower crust behave viscoelastically at a long-term scale (Lorenzo-Martin et al., 2006; Pollitz and Sacks, 2002; Zeng, 2001). Therefore, we adopted a model of dislocation sources embedded in a mixed inelastic layered half-space (Wang et al., 2006), and the code PSGRN (Wang et al., 2006) was used to compute Green's functions of a multilayered viscoelastic half-space. The layered model and the parameters that were used for our calculations are listed in Table 1, in which H is the thickness, V_P is the P wave velocity, and V_S is the S wave velocity, ρ is the density, and η is the viscosity of each layer. The values of H and V_P were obtained from a seismic study (Shen et al., 2003a,b). V_S was designated as V_P divided by $\sqrt{3}$. The density ρ was mainly based on the study of Xiong et al. (2009). Values of η were derived from the studies of Wen et al. (2012) and Zhang et al. (2007).

The static stress change is a tensor quantity, and ΔCFS depends not only on the source parameters but also on the orientation of the target fault and the slip direction on the fault. Due to the limited knowledge of the regional stress field and fault geometry, two approaches have often been used to calculate stress changes. One approach is to calculate the stress changes on optimally oriented planes (King et al., 1994; Toda et al., 1998, 2002). Another approach is to calculate the stress change on specified fault planes derived from known focal mechanisms. In this study, we used both approaches. When we focussed on the spatial correlation between seismicity and stress change, we resolved the stress changes on optimally orientated planes under a suggested regional stress regime. The study area is characterised by strike-slip faulting; thus, σ_1 and σ_3 are horizontal. Following Xu et al. (2000) the maximum stress axis is suggested to trend toward the NE40°. When we wanted to determine whether the moderate-size events of M ~5.0, whose mechanism solutions are known, were triggered by the mainshock, we used the second approach, and the plane of the target fault was suggested to be one of the nodal planes of the large aftershocks from the Harvard CMT catalogue.

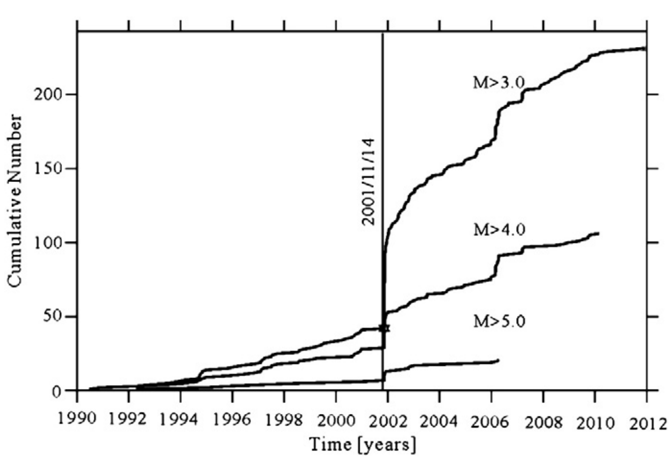

Fig. 4. Cumulative numbers of aftershocks of the 2001 great Kunlun earthquake in the studied area, January 1990–November 2011, using various cut-off magnitudes.

4.1. Slip source model

To calculate the static ΔCFS imparted by the 2001 Kunlun earthquake, we tested two variable slip source models from different data sets. The 1st slip model, from Wen et al. (2009), is derived from kinematic inversion studies using teleseismic body waveforms, together with field observations of fault slip. The 2nd slip model, from Lasserre et al. (2005), is constrained by InSAR data. Because the two models result in similar distributions of ΔCFS, results obtained using the 1st model are referenced in the present paper. Fig. 5 shows the slip distributions of this model.

Table 1
Parameters used in the layered models.

Layer	H (km)	Vp (km/s)	Vs (km/s)	ρ (kg/m^3)	η (Pa·s)
1	4.0	4.8	2.8	2600	∞
2	6.0	5.9	3.4	2700	∞
3	18.0	5.9	3.4	2850	∞
4	20.0	6.3	3.6	3000	3.0×10^{17}
5	20.0	7.1	4.1	3100	2.0×10^{19}
6	30.0	8.2	4.7	3320	2.0×10^{19}

4.2. Stress changes resolved on optimally orientated faults

Here, we focussed on the spatial correlation between seismicity and stress change. We resolved the stress changes on optimally orientated fault planes, which are constrained by the mean tectonic stress in the region mentioned in Subsection 4.1.

The 10-year catalogue of seismicity following the mainshock makes it possible to examine the triggering effect in different time spans. To obtain more detailed results, we studied three postseismic periods in order to explore the spatial correlation of seismicity and stress change. The first period consists of the 1st 200 days following the mainshock, the second period includes approximately 3 years between the end of the first time period and the end of 2005, and the third period includes six years, from 2006 through 2011.

Fig. 6a–c displays the coseismic ΔCFS from the M_s 8.1 Kunlun earthquake, with all the seismicity that was detected in the three aforementioned time spans. The stress changes were calculated on optimally oriented faults at a depth of 15 km, which was the depth of the mainshock's hypocentre and the dominant depth of the aftershocks. The red- and blue-coloured regions show positive and negative stress changes, respectively. There are four zones of stress rise and four zones of stress drop (also called stress shadows). For the long rupture plane of the mainshock, the characteristic "butterfly" pattern of static ΔCFS is not displayed. The zones at the ends of the fault extend into the fault zone, with positive stress changes, and the stress shadows on both sides of the fault are much stronger than the others.

It is clear that most of the events fall in regions of positive stress change. In particular, the seismic activity occurred at the eastern and western ends of the fault, which lie in regions of increased ΔCFS. This phenomenon is clearly visible in all three time periods, as shown in Fig. 6a–c. However, we also can observe that there are still some events located in the stress shadows. To explore the temporal evolution of the correlation between the earthquake distribution and the Coulomb stress changes, Fig. 7 shows the Coulomb stress changes calculated for individual earthquakes on an optimally oriented fault. It is clearly demonstrated that during the 1st 200 days, most earthquakes were located in a site of positive ΔCFS. However, later earthquakes do not show a very clear correlation with stress changes. Many events occurred at a larger distance, where stress changes were very small (on the order of millibars or less).

A number of factors, including crust heterogeneity, uncertainty in the source model, errors in hypocentre determination, and time-dependent behaviours of the crust and mantle, may have a role in perturbing the stress field, and thus it is not surprising that not all subsequent earthquakes occurred in regions of increased Coulomb stress. The time-dependent response is especially important for delayed aftershocks, such as were observed after the M_w 7.9 Sichuan earthquake (Lei et al., 2013). It is thus worth examining the delayed inelastic deformation in the lower crust and the upper mantle and its role in the seismicity in the study areas.

Considering the fact that the mantle and the lower crust behave viscoelastically at long-term time scales, we studied the post-seismic Coulomb stress change in only two periods: the first 4 years after the great Kunlun earthquake and the subsequent 6 years (from 2006 to 2011). Fig. 8a and b shows the stress changes estimated for given times (for 2005/12/31 and 2011/11/14, respectively), based on the viscoelastic model (Table 1), with seismicity detected in the two periods. The overall trend in Fig. 8 is that the lobe of positive stress change gradually extends to a larger area and slightly but continuously increases its amplitude over time.

Combining the results in Figs. 6–8 clearly shows that earlier seismicity is governed by coseismic stress changes.

4.3. Stress changes resolved on moderate-sized earthquakes with focal mechanisms

Figs. 6–8 provide a visual depiction of the statistical correlation between stress changes and seismicity. For earthquake hazards, however, we are also concerned about moderate-size events (of an approximate magnitude of 5.0 or greater). The mechanism solution for such event can be obtained from world-wide observations. To determine whether moderate-size events that occurred in the study area were triggered by the mainshock, we resolved the stress changes on the possible fault planes of these events.

Because we did not know which nodal plane was the rupture plane, we calculated the stress changes on two nodal planes. We obtained focal mechanism solutions for 24 events from the Harvard CMT catalogue, as listed in Table 2, where ΔCFS_1 and ΔCFS_2 are the coseismic ΔCFS resolved on the first and second nodal planes, respectively, and ΔCFS_3 and ΔCFS_4 are the post-seismic ΔCFS calculated using the multi-layered viscoelastic half-space model of Table 1 on the first and second nodal planes, respectively. It should be noted that ΔCFS_3 and ΔCFS_4 are provided at the origin time of each event. If we artificially select the nodal plane with the larger ΔCFS value as the source fault plane, the results reveal that 19 out of 24 events have a positive coseismic stress change induced by the mainshock, and the values of coseismic stress change for the early events are larger than for later events. It is worth noting that the effect of viscoelastic relaxation is not obvious for the early events, and the stress changes for most of early events are decreased by the inelastic response. However, the value of the post-seismic Coulomb stress is obviously larger than the coseismic stress change for recent events (since 2006), indicating the growing importance of the inelastic response. This result again demonstrates that earlier seismicity is governed by coseismic stress changes and shows that the effects of post-seismic stress changes due to inelastic response become gradually more obvious since 2006.

4.4. ETAS modelling analysis

It is known that the seismic triggering process may be complicated by a number of factors, such as fractal fault systems and the fact that any earthquake can trigger its own aftershocks. Statistical approaches are thus important. Anomalies in seismicity have been suggested as important indicators for evaluating the effects of stress changes (Husen et al., 2004; Husker and Brodsky, 2004; Lei et al., 2011; Ogata, 2005, 2011; Ogata et al., 2003; Pankow et al., 2004). In this section, we relate stress changes to seismicity rate changes using the epidemic type aftershock sequence (ETAS) model (Lei et al., 2008, 2011; Ogata, 2005, 2011).

The ETAS model incorporates the Omori law by assuming that every aftershock can trigger its own aftershocks. Additionally, the occurrence rate is described as the sum of the aftershock rate related to all

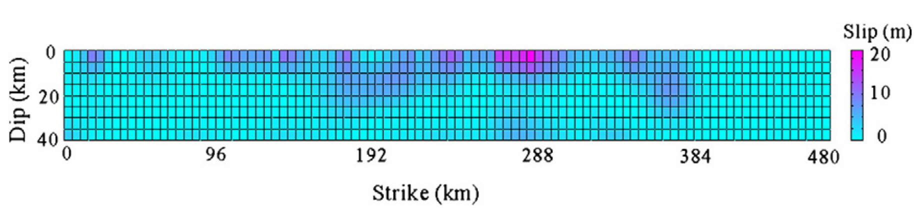

Fig. 5. Slip distributions of the M_s 8.1 Kunlun earthquake according to Wen et al. (2009). The total rupture plane is set to a length of 480 km and a width of 40 km, which is discretised as a set of 768 square patches of dimension of 5×5 km^2.

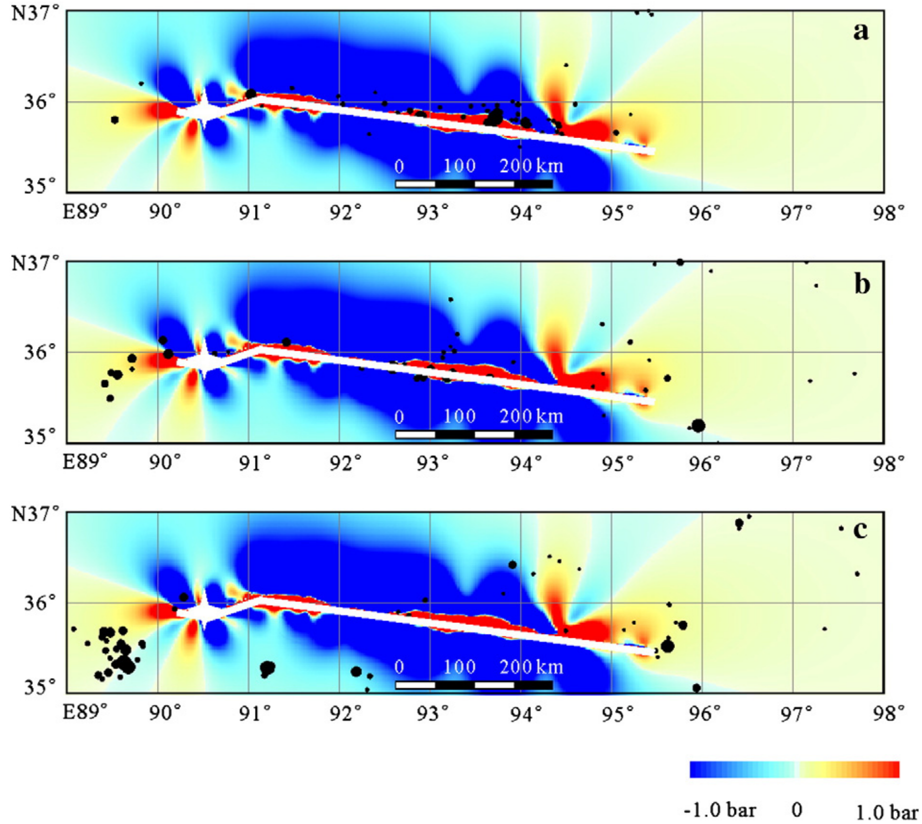

Fig. 6. Coseismic Coulomb stress changes calculated at a 15-km depth using the slip model proposed by Wen et al. (2009). Stress is resolved on optimally oriented faults. Panels (a), (b), and (c) show the Coulomb stress changes calculated in an elastic half-space and seismic activities occurring in the three post-seismic periods. The white star near the west end of the rupture indicates the M_s 8.1 mainshock, and the black circles scaled by magnitude denote seismicity occurring in different time spans. The thick white lines show the projection of the (nearly vertical) rupture plane on the surface. These calculations were performed using GeoTaos software (http://staff.aist.go.jp/xinglin-lei).

preceding earthquakes and a constant rate p_0 that represents the random background activity with a Poisson distribution:

$$\lambda(t) = p_0 + \sum_{i}^{t_i<t} K_0 (t - t_i + c)^{-p} 10^{\alpha(M_i - M_c)}. \quad (1)$$

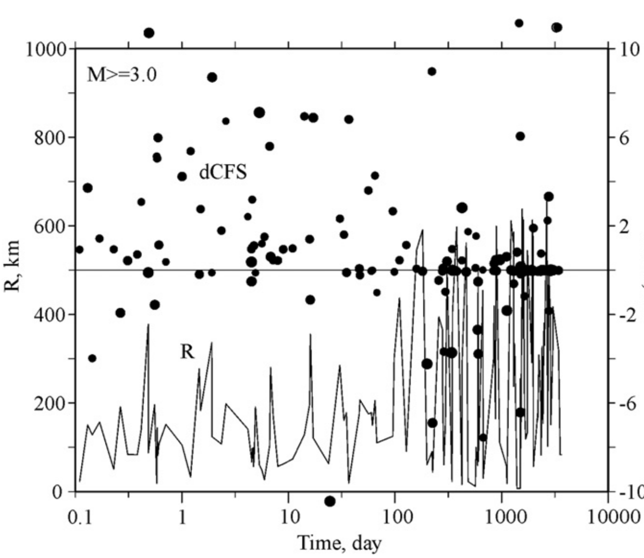

Fig. 7. Coseismic Coulomb stress changes calculated for individual earthquakes on an optimally oriented fault. R indicates the distance of the hypocentre from the mainshock.

M_i and M_c represent the magnitude of the ith earthquakes and the cut-off magnitude, respectively. P_0, K_0, c, α and p are empirical parameters. All these parameters for the dataset are estimated by minimising the Akaike information criterion (AIC) (Akaike, 1974). If the estimated model is correct, the cumulative number becomes a Poisson process on the transformed time, defined as $\int \lambda(t)dt$. It is convenient to give the relative percentage of the random component over the total occurrence rate on a time interval [S, T] (Lei et al., 2008):

$$R(\%) = 100 p_0 (T - S) / \int_S^T \lambda(d)dt. \quad (2)$$

Given a series of earthquakes, one can apply the ETAS model to the data set and calculate the predicted cumulative curve for any given period. For a narrow study zone, the ETAS model is fitted to the sequence of earthquakes in either the entire period or a number of separated periods, in order to identify significant change points. After the change point, the actual cumulative number is compared to the theoretical cumulative cure of the ETAS model. If the actual cumulative number deviates upward from the expected values, this suggests an activation period relative to the ETAS model. If the actual cumulative curve deviates downward, this suggests a quiescent period relative to the model (Ogata, 2005, 2011). The presence of significant activation or quiescence relative to the ETAS model is a stress change sensor (Helmstetter and Sornette, 2003a; Ogata, 2005, 2011; Ogata et al., 2003).

As shown in Figs. 6 and 7, most events of the 2001 Kunlun earthquake occurred in the neighbouring area of the rupture plane of the mainshock and were found in regions of positive stress change. We directly applied the ETAS model to the earthquake sequence that occurred in the entire study area during the period Jan. 1990–Nov. 2011.

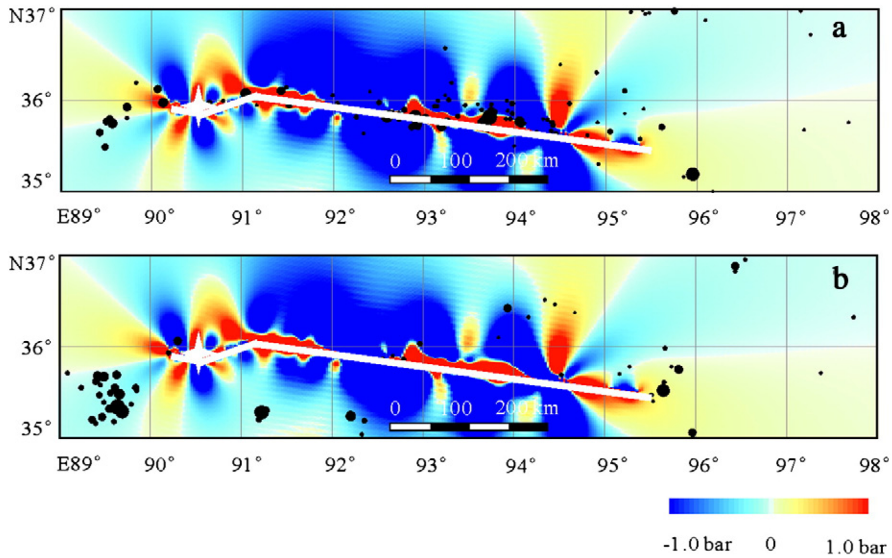

Fig. 8. Post-seismic ΔCFS at 15 km depth. Stress is resolved on optimally oriented faults under the suggested stress regime. (a) ΔCFS at the end of 2005 with seismicity for the period 2001–2005. (b) ΔCFS on 2011/11/14, with seismicity for the period from 2006 to 2011/11/14.

Fig. 9 provides a summary of the results of the ETAS analyses. As shown in Fig. 9a and b, two major change points can be found, dividing the earthquake sequence into three phases. The two change points were determined to be Nov. 2001 and March 2006, according to the method of Ogata et al. (2003). The three-band ETAS model of the phases, divided at the change points (Fig. 9c–e), fits better than the single ETAS model for the whole period (Fig. 9b). The ETAS parameters for phase I are in the range of typical tectonic earthquakes. In the later phases, the ETAS models show small α values of 1.637 and 1.490 for phases II and III (Fig. 9d and e), respectively. A low value for α generally suggests more swarm-like seismicity, which is distinguishable from the background seismicity (Lei et al., 2008; Ogata, 1999). Fig. 9 shows that the seismicity change in the study area had a close association with the 2001 Kunlun earthquake, and the first change point corresponds to the occurrence of the M_s 8.1 Kunlun earthquake. We also see the actual cumulative numbers of events deviating upward from the theoretical cumulative curve, showing activation relative to the ETAS model (Fig. 9d), which is in agreement with the positive increment of stress changes. After the second change point in 2006, there was no significant change in seismicity up to the end of the study period.

Up to this point, we can draw the following conclusive results: 1) static ΔCFS has a strong effect on short-term (up to 200 days in our case) seismic triggering; and 2) ETAS modelling and other statistics demonstrate that the present-day seismicity has decreased to the level of background seismicity before the great earthquake, and long-term seismic triggering plays a role for over 10 years. By linking the earthquake occurrence model with the Coulomb stress change, we can make a rough estimate of the decay of seismic rate raised by a small step of the loading, following the seismicity rate equation given by Dieterich (1994):

$$R(t) = \frac{r}{\left[\exp\left(\frac{-\Delta CFS}{A\sigma}\right) - 1\right]\exp\left(\frac{-t}{t_a}\right) + 1} \quad (3)$$

where $R(t)$ is the seismicity rate after a transient stress change, r is the background seismicity rate, ΔCFS is the Coulomb failure stress change, A is a dimensionless fault constitutive parameter, and σ is the effective normal stress. The parameter t_a represents the characteristic time of aftershock duration. If all parameters are known, the ratio of the seismicity rate $R(t)/r$ varies with the static stress changes. Parsons (2002) found that $t_a = 7$–11 years for 100 M >7 global earthquakes. We assumed that t_a was 10 years in our estimate. In addition, we suggest that $A\sigma = 0.1$ bar, following Toda et al. (2008). For estimating the aftershock duration by a given value of ΔCFS, we assumed that the increased seismic activity drops to a level of 10%, that is to say, we used the time t_f, with $R(t_f)/r = 1.1$ considered to be the duration of the triggering effect for a given amplitude of static stress change. As a result, we find that t_f ranges from 0.5 year to 24 years for ΔCFS amplitudes from 0.01 to 10.0 bars. These are the major values of positive stress change that are correlated with regions of aftershocks, as shown in Fig. 7. Thus, the M_s 8.1 Kunlun earthquake may affect local seismicity for days to tens of years.

5. Long-term evolution of stress changes along the Kunlun fault system

Together with the 2001 M_s 8.1 earthquake, a sequence of five large earthquakes of M ≥7.0 have ruptured different segments of the Kunlun fault system since 1937 (Fig. 1). Because some highly populated cities, such as Golmud, are close to the Kunlun fault, an improved understanding of the evolution of stress along the Kunlun fault system and changes in local seismicity is therefore important for seismic hazard assessment in this region.

Recently, Xiong et al. (2009) investigated the evolution of stress changes for an earthquake sequence of M ≥7.0 by resolving the stress change on the fault plane of the next event. Considering the long time span (several decades), the effect of tectonic stress cannot be neglected when evaluating the evolution of stress along the Kunlun fault system. Therefore, we calculated the stress changes that were due to tectonic loading and to previous earthquakes.

The source parameters of the five large earthquakes in our calculation use the same values that were listed in Table 1 of Xiong et al. (2009), except that a simple rupture model with an average slip displacement of 3.0 m is used for the 1997 Manyi earthquake. Other parameters and the viscoelastic model used in the calculation of the Coulomb stress changes are the same as we previously mentioned in Section 4. We estimated the tectonic stress loading using a deep steady slip model, following the method applied to the North Anatolian fault (Stein et al., 1997). According to the results of Van der Woerd et al. (2000, 2001, 2002), the long-term slip rate is 11.5 ± 2 mm/year along much of the Kunlun fault. An additional study at a site near ~92°E (Li et al., 2005) suggests a slip rate of 10 ± 1.5 mm/year. The easternmost segment of the Kunlun fault exhibits slip rates of 2 to 6 mm/year (Kirby et al., 2007). Bell et al. (2011) estimated a slip rate of 3 ± 2 mm/year along the Manyi fault. Based on these estimates of the geological slip

Table 2
Parameters and stress changes for 24 moderate-size events.

No.	Date	Epicentre (Harvard)			M_w	Nodal plane 1			Nodal plane 2			ΔCFS_1 (bars)	ΔCFS_2 (bars)	ΔCFS_3 (bars)	ΔCFS_4 (bars)
	(UTC)	Long. (deg)	Lat. (deg)	Depth (km)		Strike (deg)	Dip (deg)	Rake (deg)	Strike (deg)	Dip (deg)	Rake (deg)				
1	2001/11/18	93.51	35.94	15.0	5.6	282	40	112	74	54	72	−0.11	−1.32	−0.10	−1.16
2	2001/11/19	93.52	35.83	15.0	5.3	100	44	90	280	46	90	−1.23	3.91	−1.33	3.78
3	2001/11/30	91.11	36.07	15.0	5.2	187	34	−149	71	74	−60	11.39	18.17	11.10	18.01
4	2001/12/01	93.93	35.58	15.0	5.1	254	36	−141	131	69	−61	1.73	1.11	1.94	1.18
5	2001/12/08	93.13	36.07	15.0	5.2	89	30	−40	216	71	−113	−6.10	−5.74	−5.88	−5.67
6	2002/10/19	92.87	35.72	33.0	5.1	186	76	−166	92	76	−14	2.94	1.54	2.55	1.11
7	2002/10/26	96.14	35.18	33.0	5.3	11	78	176	101	86	12	0.05	0.02	0.04	0.03
8	2004/06/29	92.54	35.75	17.1	5.3	93	63	−15	190	76	−152	−3.58	−4.56	−3.21	−4.08
9	2004/12/10	93.35	35.83	19.4	5.0	341	48	133	106	57	52	−2.92	−8.35	−2.22	−7.71
10	2005/06/01	89.56	35.70	21.4	4.9	343	69	−161	246	72	−22	0.16	0.31	0.14	0.33
11	2006/02/26	89.67	35.36	12.0	5.4	158	61	−150	52	64	−33	0.12	0.25	0.21	0.39
12	2006/03/01	89.67	35.40	18.6	5.1	60	50	−31	171	67	−136	0.11	0.25	0.17	0.39
13	2006/03/29	95.62	35.53	24.3	5.3	297	73	11	204	79	163	0.09	0.21	0.09	0.29
14	2006/04/14	89.74	35.46	17.7	5.6	353	49	−137	231	59	−50	0.08	0.28	0.19	0.41
15	2006/09/01	89.62	35.35	23.6	4.8	12	39	−105	211	53	−78	0.12	0.19	0.23	0.29
16	2007/03/15	89.49	35.50	18.6	5.0	41	46	−51	172	56	−123	0.20	0.23	0.29	0.36
17	2007/03/16	89.50	35.56	16.5	5.0	41	45	−47	168	59	−124	0.22	0.26	0.31	0.40
18	2007/04/09	89.51	35.50	20.8	4.9	36	47	−56	171	53	−121	0.22	0.23	0.32	0.36
19	2008/06/18	91.33	35.31	22.5	5.4	252	88	0	162	90	178	−0.16	0.20	−0.11	0.44
20	2008/10/20	91.32	35.26	22.9	5.0	341	86	−177	251	87	−4	−0.16	0.19	−0.10	0.43
21	2009/06/21	90.31	36.05	18.2	4.9	349	85	−175	259	85	−5	−2.11	−2.71	−1.92	−2.67
22	2009/09/28	95.90	35.82	24.4	4.8	178	61	178	269	88	29	0.07	0.13	0.10	0.25
23	2009/10/16	92.34	35.17	20.6	4.9	309	79	179	40	89	11	0.20	0.79	0.32	0.89
24	2010/02/23	91.30	35.30	23.9	4.8	343	85	176	74	86	5	−0.15	0.22	−0.09	0.42
Number of +ΔCFS												15	19	15	19
Number of −\ ΔCFS												9	5	9	5

rate, the slip rate along the Kunlun fault system is assumed to increase from 0 at a 20-km depth to the full rate at a 100-km depth in our slip model.

Fig. 10 shows the evolution of post-seismic stress changes due to the historic sequence of large earthquakes along the Kunlun fault. The red- and blue-coloured regions show positive and negative stress changes, respectively. Stress is resolved on the fault plane of the next event. Fig. 10 shows that all the subsequent events of M ≥7.0 occurred in regions of positive ΔCFS, which contains stress changes due to all previous events. This feature may conclusively reveal the long-term triggering effect for these M ≥7.0 events along the Kunlun fault system under the influence of viscoelastic relaxation. The spatial distribution of the stress changes shows a left-lateral feature, which is consistent with focal mechanisms of these M ≥7.0 events. The reason for this observation is hypothesised as follows. The Kunlun fault system contains several major segments. A step-over generally develops between neighbouring segments. Seismic ruptures are generally initiated at one step-over and terminate at another, causing large stress changes at the step-overs that promote the rupture of neighbouring segments.

Fig. 11a displays the stress accumulation over 74 years of tectonic loading (from 1937 to 2011), and Fig. 11b shows the post-seismic Coulomb stress field from 1937 to 2011. It is worth noting that the stress evolution due to tectonic loading and viscoelastic relaxation controls future seismic activities. Figs. 10 and 11 show that earthquake-induced stress increases of several bars in the vicinity promoted the Kunlun earthquake sequence and that each shock increased the probability of future earthquakes at the site of the next strike. Moreover, we see that the amplitude of positive Coulomb stress changes slightly increases over time, and the effect of post-seismic viscoelastic relaxation is more obvious than that of tectonic loading along the Kunlun fault system. This can be easily understood by noting that as viscoelastic flow relaxes, it carries the stress from the lower crust and upper mantle to the upper crust.

As shown in Fig. 11, the state of the stress field for the regions along the Kunlun fault is subject to the combined effects of M ≥7.0 earthquakes. Some zones show accumulating stress rise, and some zones show a decrease in stress. Fig. 11 shows that segments A and B are located in the regions of accumulating stress rise. Because the M ≥7.0 events along the Kunlun fault generally possess a left-lateral distribution, segment B may therefore have the highest potential for seismic hazard in the future.

6. Discussion

Here we discuss major factors that may cause uncertainties in our numerical results. According to the static stress triggering hypothesis, uncertainty in all the suggested parameters may produce uncertainty in the stress calculations. The major factors include inhomogeneity of the crust, viscosity, the use of the slip model for large earthquakes, the location of the hypocentre, and the regional stress regime.

Changes in viscosity may affect these results. According to studies of post-seismic deformation and rheological properties (Shen et al., 2003a; Wen et al., 2012), flow of the mid-crust in the Tibetan Plateau requires the lower crust to have low viscosity, and different methods have estimated viscosity in this region to range from 10^{16} to 10^{21} Pa·s. Here, we assumed that the lower crust or mantle has this range of viscosity values, and we examined the range of stress changes and tested the stability of the results. To examine the effect of uncertainty regarding viscosity, we changed the viscosities in Layers 4–6 of the model (Table 1) from the order of 10^{16} to the order of 10^{21} but maintained fixed original values in the other layers. For example, we calculated the stress changes induced by the 2001 Kunlun mainshock on the first nodal plane of the fourth event in Table 2. The resulting contribution to the time-dependent stress changes is on the order of 0.001–0.01 bar, which is a minor deviation and does not seriously affect our results.

At least five slip models of the 2001 Kunlun earthquake have been proposed in previous studies, two of which (Lasserre et al., 2005; Wen et al., 2009) were determined not only from teleseismic waves but also from field observations or InSAR data. The first model (Lasserre et al., 2005) is divided into two fault sections, with the largest slip occurring at depths between 0 and 5 km and reaching ~8 m in two areas. In the second model (Wen et al., 2009), the spatial slip distribution along the fault was divided into five segments, and the largest rupture velocity (of approximately 6 km/s) occurred in the third and fourth segments.

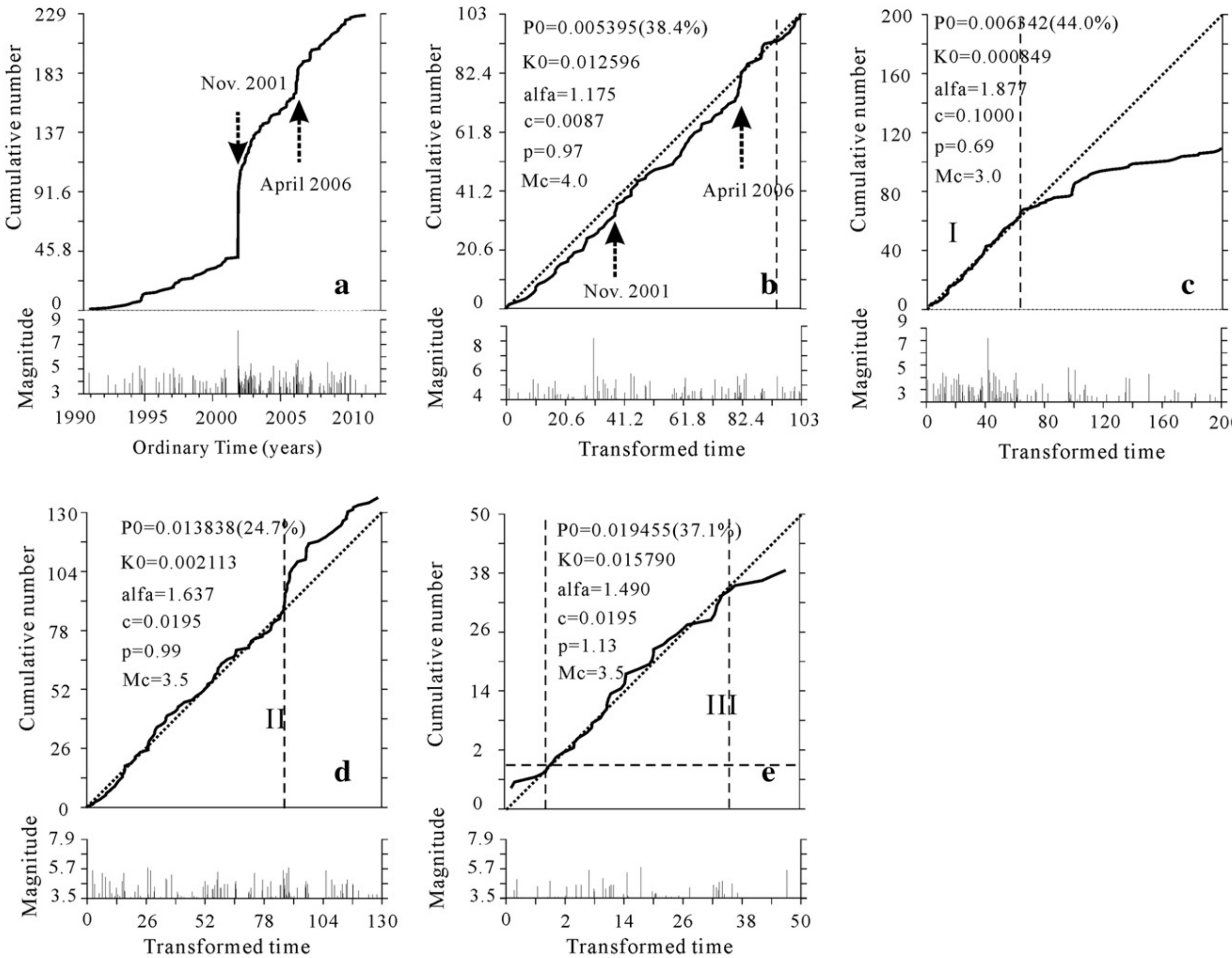

Fig. 9. The cumulative number and magnitude of the Kunlun earthquake sequence for the period 1990 through November 2011. Panels (a) and (b) show a single ETAS model applied to the whole period, and panels (c)–(e) show a three-stage ETAS model applied separately to the three phases. Fig. 9a plots the cumulative number versus ordinary time, whereas Fig. 9b–e plots the cumulative number against transformed time. The dotted and inclined line indicates the theoretical cumulative number predicted by the ETAS model, and the curve indicates the actual cumulative number in the different time scales. The dotted and vertical line shows the data range for the ETAS estimate in each phase. The arrow indicates the change point.

We applied these two models in order to conduct a comparison study and found that the stress changes calculated by the model of Wen et al. (2009) were lower than those calculated using the model of Lasserre et al. (2005) in the near-field. This difference may be due to the fact that Wen's model included fewer subfaults with larger slip than the model of Lasserre et al. However, the two models result in similar distributions of Coulomb stress changes. Moreover, the difference in the resulting stress amplitude decreases with increasing distance from the mainshock, which applies to the evolution of stress changes due to the historic sequence of large earthquakes. Therefore, the basic results presented in this paper would not change much when the different existing slip models are used.

Our work is an example of studies of the short- and long-term earthquake triggering along a long strike-slip fault system, using the earthquake catalogue obtained by the China Earthquake Data Centre. The minimum magnitude of completeness is 4.0 for the period from 1990 through 2000 and 3.5 for the later period. In other words, some earthquakes with magnitudes less than 4.0 or 3.5 are not detected by the local seismic network. Generally, due to their large number, small earthquakes are important for examining statistical significance when analysing earthquake triggering, especially in the ETAS modelling analysis. Thus, our results are limited for earthquakes of a magnitude greater than 3.5.

Our objective was to examine the correlation between changes in Coulomb stress and changes in seismicity rate and to study the detailed features of seismic triggering following the M_s 8.1 Kunlun earthquake. A clear correlation between stress changes and seismicity distribution was detected through statistical analyses of Coulomb stress changes. The present study provides evidence that the M_s 8.1 Kunlun mainshock triggered both short-term aftershocks and long-term seismic activity through effects on both viscoelastic relaxation and other inelastic responses. The clearest seismic triggering imparted by the M_s 8.1 Kunlun earthquake was during the 1st 200 days after the earthquake, but seismic triggering persisted until 2010. Since then, seismic activity, at least for $M \geq 3.5$, has decreased to levels near the pre-Kunlun-earthquake background rate.

During the first several years after the earthquake, triggered seismic activities occurred primarily at sites adjacent to the eastern segment of the ruptured fault, corresponding with areas of positive coseismic stress changes. Subsequent events clustered close to the western segment of the ruptured fault. It is worth noting that since 2006, a dense seismic cluster has formed in the large junctional region between the Manyi fault and the Kunlun earthquake source fault. Consistent with this spatial distribution, ETAS analysis also shows a clear change point of seismic activity in 2006. This junction is an extensive one due to the left-lateral slip features of the adjusted faults. Such zones may act as paths of localised flow in the middle crust for fluids derived from deep level over-pressured reservoirs (Lei et al., 2011). Indeed, this junction is characterised by high geothermal flux and hot springs (http://wenku.baidu.com/view/d80095f5ba0d4a7302763af4.html). The ETAS model of phase III (2006–2011) with a low value of α (Fig. 10) may be a sign of fluid, however further studies are needed to address this interesting issue.

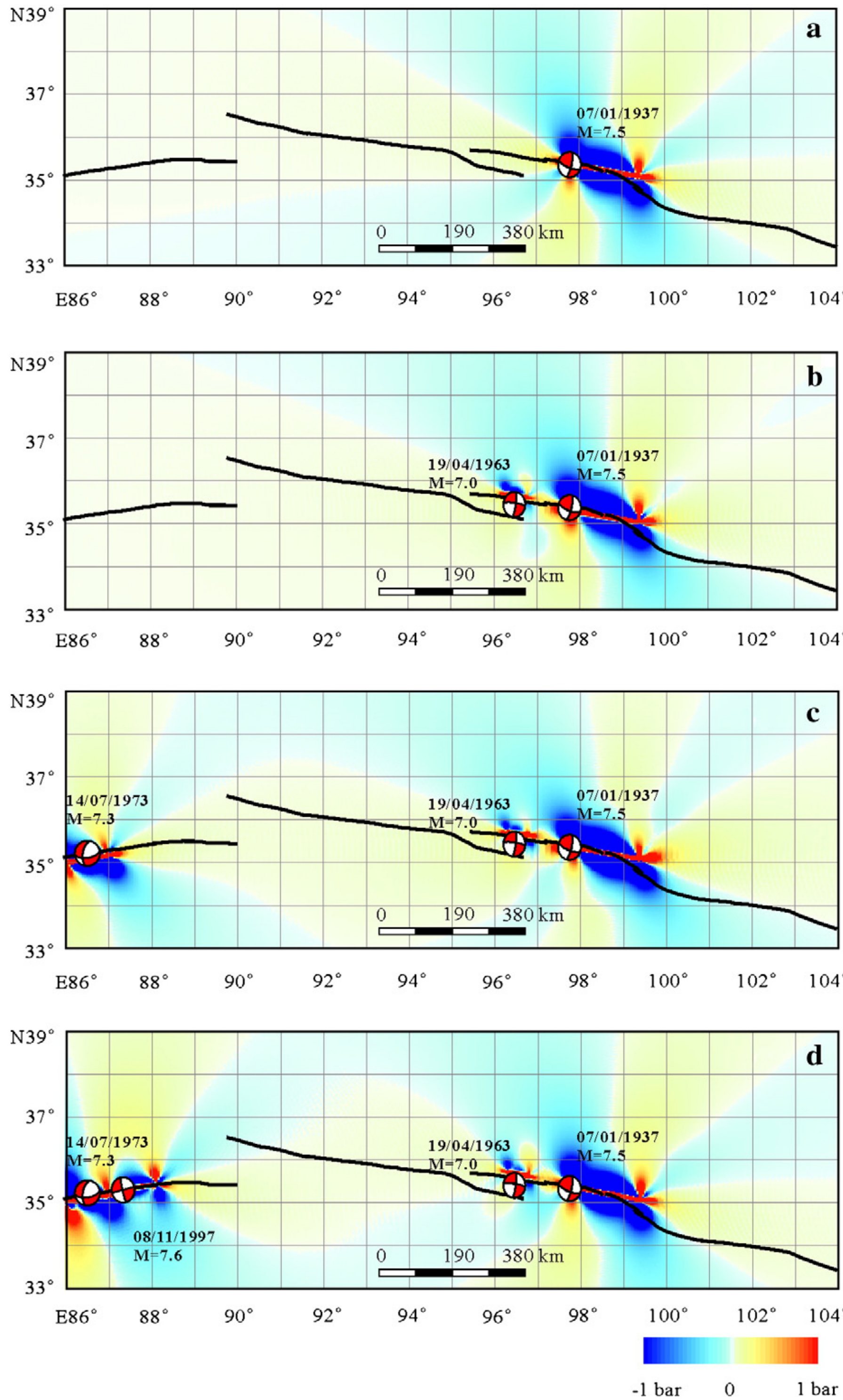

Fig. 10. Evolution of the accumulated post-seismic stress changes at a 10-km depth associated with the four M ≥7.0 earthquakes occurring along the Kunlun fault before 2001. Stress is resolved on the fault plane of the next event. Beach balls show the locations and focal mechanisms of the M ≥7.0 earthquakes, and the black lines are segments of the Kunlun fault.

7. Conclusions

By comparing time-dependent stress changes and seismicity after the 2001 M_s 8.1 Kunlun earthquake, we can conclude that short-term seismic triggering, which corresponds to the most intensive period of aftershock activity, is governed by coseismic stress changes. Post-seismic Coulomb stress changes due to viscoelastic relaxation have an increasing role in long-term seismic triggering. The background effect of tectonic loading should certainly not be ignored.

Furthermore, we discuss long-term triggering and the evolution of stress changes for the sequence of the five large earthquakes (of M ≥7.0) that have ruptured the Kunlun fault system since 1937. All subsequent events of M ≥7.0 occurred in the regions exhibiting positive ΔCFS that accumulated from previous earthquakes. We find that the stress

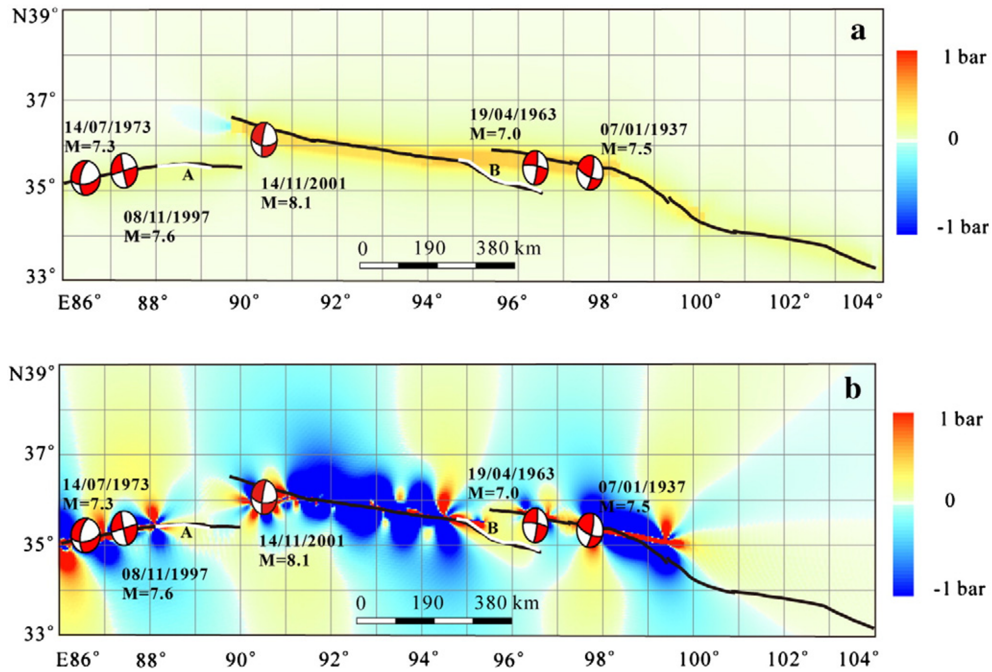

Fig. 11. Distributions of earthquake epicentres and stress changes at a 10-km depth over 74 years of tectonic loading from 1937 to 2011. Panel (a) shows accumulated stress evolution from the five M ≥ 7.0 earthquakes under complete viscoelastic relaxation from 1937 to 2011. Panel (b) shows that stress is resolved on optimally oriented faults. Beach balls show the locations and focal mechanisms of the M ≥ 7.0 earthquakes, and the black lines are segments of the Kunlun fault. The white lines show the two fault segments that are highlighted in our study.

evolution due to the viscoelastic relaxation of stress caused by previous large events controls the occurrence of the next large earthquakes along the Kunlun fault, which has been continuously stressed by tectonic loading. The fact that five large earthquakes occurred sequentially within 70 years, a significantly shorter period than the repeating period (several thousands of years) of large earthquakes along the Kunlun fault that is estimated by the tectonic loading rate, demonstrates the importance of delayed triggering governed by viscoelasticity. Long-term earthquake triggering may simply reflect the prolonged or delayed nature of the triggering process. Our results suggest that earthquakes interact and that when a large shock occurs, it changes the conditions for failure in its vicinity, altering the probability of future events.

Acknowledgements

This work was supported by the National Natural Science Foundation of China (Grant No. 41104036). We appreciate the help of R. J. Wang, C. Lasserre and Yi-Ying Wen. We thank the associate editor and two anonymous reviewers for providing numerous comments that significantly improved the manuscript.

References

Akaike, H., 1974. A new look at the statistical model identification. IEEE Trans. Autom. Control 19, 716–723. http://dx.doi.org/10.1109/TAC.1974.1100705.

Anderson, G., Johnson, H., 1999. A new statistical test for static stress triggering: application to the 1987 Superstition Hills earthquake sequence. J. Geophys. Res. 104, 20153–20168.

Bell, M.A., Elliott, J.R., Parsons, B.E., 2011. Interseismic strain accumulation across the Manyi fault (Tibet) prior to the 1997 M_w 7.6 earthquake. Geophys. Res. Lett. 38, L24302. http://dx.doi.org/10.1029/2011GL049762.

Brodsky, E.E., Karakostas, V., Kanamori, H., 2000. A new observation of dynamically triggered regional seismicity: earthquakes in Greece following the August, 1999 Izmit, Turkey earthquake. Geophys. Res. Lett. 27, 2741–2744.

Caskey, S.J., Wesnousky, S.G., 1997. Static stress changes and earthquake triggering during the 1954 Fairview Peak and Dixie Valley earthquakes, central Nevada. Bull. Seismol. Soc. Am. 87, 521–527.

Catalli, F., Cocco, M., Console, R., Chiaraluce, L., 2008. Modeling seismicity rate changes during the 1997 Umbria–Marche sequence (central Italy) through a rate- and state-dependent model. J. Geophys. Res. 113. http://dx.doi.org/10.1029/2007JB005356 (B11301).

Dieterich, J., 1994. A constitutive law for rate of earthquake production and its application to earthquake clustering. J. Geophys. Res. 99, 2601–2618.

Felzer, K.R., Becker, T.W., Abercrombie, R.E., Ekström, G., Rice, J.R., 2002. Triggering of the 1999 M_w 7.1 Hector Mine earthquake by aftershocks of the 1992 M_w 7.3 Landers earthquake. J. Geophys. Res. 107. http://dx.doi.org/10.1029/2001JB000911.

Fu, B., Awata, Y., Du, J., Ninomiya, Y., He, W., 2005. Complex geometry and segmentation of the surface rupture associated with the 14 November 2001 great Kunlun earthquake, northern Tibet, China. Tectonophysics 407, 43–63.

Gomberg, J., Beeler, N.M., Blanpied, M.L., 1998. Earthquake triggering by transient and static deformations. J. Geophys. Res. 103, 24411–24426.

Gu, G., Lin, T., Shi, Z., 1989. Catalogue of Chinese Earthquakes (1831 BC–1969 AD). Science Press, Beijing.

Harris, R.A., 1998. Introduction to special section: stress triggers, stress shadows, and implications for seismic hazard. J. Geophys. Res. 103, 24347–24358.

Helmstetter, A., Sornette, D., 2003a. Mainshocks are aftershocks of conditional foreshocks: how do foreshock statistical properties emerge from aftershock laws. J. Geophys. Res. 108 (B1), 2046. http://dx.doi.org/10.1029/2002JB001991.

Helmstetter, A., Sornette, D., 2003b. Bath's law derived from the Gutenberg–Richter law and from aftershock properties. Geophys. Res. Lett. 30, 2069. http://dx.doi.org/10.1029/2003GL018186.

Husen, S., Wiemer, S., Smith, R.B., 2004. Remotely triggered seismicity in the Yellowstone National Park region by the 2002 M_w 7.9 Denali fault earthquake, Alaska. Bull. Seismol. Soc. Am. 94, S317–S331.

Husker, A.L., Brodsky, E.E., 2004. Seismicity in Idaho and Montana triggered by the Denali fault earthquake: a window into the geologic context for seismic triggering. Bull. Seismol. Soc. Am. 94, S310–S316.

Kilb, D., Gomberg, J., Bodin, P., 2002. Aftershock triggering by complete Coulomb stress changes. J. Geophys. Res. 107. http://dx.doi.org/10.1029/2001JB000202.

King, G.C.P., Stein, R.S., Lin, J., 1994. Static stress changes and the triggering of earthquakes. Bull. Seismol. Soc. Am. 84, 935–953.

Kirby, E., Harkins, N., Wang, E., et al., 2007. Slip rate gradients along the eastern Kunlun fault. Tectonics 26. http://dx.doi.org/10.1029/2006TC002033 (TC2010).

Klinger, Y., Xu, X., Tapponnier, P., Van der Woerd, J., Lasserre, C., King, G., 2005. High-resolution satellite imagery mapping the rupture and slip distribution of the M_w = 7.8, November 14, 2001 Kokoxili earthquake (Kunlun, Tibet, China). Bull. Seismol. Soc. Am. 95 (5), 1970–1987.

Lasserre, C., Peltzer, G., Klinger, Y., Van Der Woerd, J., Tapponnier, P., 2005. Coseismic deformation of the 2001 M_w = 7.8 Kokoxili earthquake in Tibet, measured by synthetic aperture radar interferometry. J. Geophys. Res. 110. http://dx.doi.org/10.1029/2004JB003500 (B12408).

Lei, X.L., Yu, G., Ma, S., Wen, X., Wang, Q., 2008. Earthquakes induced by water injection at 3 km depth within the Rongchang gas field, Chongqing, China. J. Geophys. Res. 113. http://dx.doi.org/10.1029/2008JB005604 (B10310).

Lei, X.L., Xie, C.D., Fu, B.H., 2011. Remotely triggered seismicity in Yunnan, southwestern China, following the 2004 M_w9.3 Sumatra earthquake. J. Geophys. Res. 116, B08303. http://dx.doi.org/10.1029/2011JB008245.

Lei, X.L., Ma, S., Su, J., Wang, X., 2013. Inelastic triggering of the 2013 Mw6.6 Lushan earthquake by the 2008 Mw7.9 Wenchuan earthquake. Seismol. Geol. 35 (2). http://dx.doi.org/10.3969/j.issn.0253-4967.2013.02.019.

Li, H., Van der Woerd, J., Tapponnier, P., et al., 2005. Slip rate on the Kunlun fault at Hongshui Gou, and recurrence time of great events comparable to the 14/11/2001, Mw 7.9 Kokoxili earthquake. Earth Planet. Sci. Lett. 237, 285–299.
Lin, A., Guo, J., Kano, K., Awata, Y., 2006. Average slip-rate and recurrence interval of large magnitude earthquake along the western segment of the Kunlun fault, northern Tibet. Bull. Seismol. Soc. Am. 96, 1597–1611.
Lorenzo-Martin, F., Roth, F., Wang, R.J., 2006. Elastic and inelastic triggering of earthquakes in the North Anatolian Fault zone. Tectonophysics 424 (3–4), 271–289.
Marsan, D., 2003. Triggering of seismicity at short timescales following Californian earthquakes. J. Geophys. Res. 108. http://dx.doi.org/10.1029/2002JB001946.
Molnar, P., Deng, Q.D., 1984. Faulting associated with large earthquakes and the average rate of deformation in central and eastern Asia. J. Geophys. Res. 89 (B7), 6203–6227.
Molnar, P., Lyon-Caen, H., 1989. Fault plane solutions of earthquakes and active tectonics of the Tibeteau and its margins. Geophys. J. Int. 99, 123–153.
Moran, S.C., Power, J.A., Stihler, S.D., Sanchez, J.J., Caplan-Auerbach, J., 2004. Earthquake triggering at Alaskan volcanoes following the 3 November 2002 Denali Fault earthquake. Bull. Seismol. Soc. Am. 94, S300–S309.
Ogata, Y., 1999. Seismicity analysis through point-process modeling: a review. Pure Appl. Geophys. 155, 471–507. http://dx.doi.org/10.1007/s000240050275.
Ogata, Y., 2005. Detection of anomalous seismicity as a stress change sensor. J. Geophys. Res. 110. http://dx.doi.org/10.1029/2004JB003245 (B05S06).
Ogata, Y., 2011. Pre-seismic anomalies in seismicity and crustal deformation: case studies of the 2007 Noto Hanto earthquake of M6.9 and the 2007 Chuetsu-oki earthquake of M6.8 after the 2004 Chuetsu earthquake of M6.8. Geophys. J. Int. 186, 331–348. http://dx.doi.org/10.1111/j.1365-246X.2011.05033.x.
Ogata, Y., Jones, L.M., Toda, S., 2003. When and where the aftershock activity was depressed: contrasting decay patterns of the proximate large earthquakes in southern California. J. Geophys. Res. 108 (B6), 2318. http://dx.doi.org/10.1029/2002JB002009.
Okada, Y., 1992. Internal deformation due to shear and tensile faults in a half-space. Bull. Seismol. Soc. Am. 82, 1018–1040.
Pankow, K.L., Arabasz, W.J., Pechmann, J.C., Nava, S.J., 2004. Triggered seismicity in Utah from the 3 November 2002 Denali Fault earthquake. Bull. Seismol. Soc. Am. 94, S332–S347.
Parsons, T., 2002. Global Omori law decay of triggered earthquakes: large aftershocks outside the classical aftershock zone. J. Geophys. Res. 107 (B9), 2199–2218.
Pollitz, F.F., Sacks, I.S., 2002. Stress triggering of the 1999 Hector Mine earthquake by transient deformation following the 1992 Landers earthquake. Bull. Seismol. Soc. Am. 92 (4), 1487–1496. http://dx.doi.org/10.1785/0120000918.
Reasenberg, P.A., Simpson, R.W., 1992. Response of regional seismicity to the static stress change produced by the Loma Prieta earthquake. Science 255, 1687–1690.
Shen, Z.K., Wan, Y.G., Gan, W.J., Zeng, Y.H., Reng, Q., 2003a. Viscoelastic triggering among large earthquake along the east Kunlun fault system. Chin. J. Geophys. 46 (6), 786–795 (in Chinese with English abstract).
Shen, Z.K., Zeng, Y., Wang, M., et al., 2003b. Postseismic Deformation Modeling of the 2001 Kokoxili Earthquake, Western China. EGS-AGU-EUG Joint Assembly, Nice, France, April.
Stein, R.S., 1999. The role of stress transfer in earthquake occurrence. Nature 402, 605–609.
Stein, R.S., King, G.C.P., Lin, J., 1992. Change in failure stress on the southern San Andreas fault system caused by the 1992 magnitude = 7.4 Landers earthquake. Science 258, 1328–1332.
Stein, R.S., King, G.C.P., Lin, J., 1994. Stress triggering of the 1994 M = 6.7 Northridge, California, earthquake by its predecessors. Science 265, 1432–1435.
Stein, R.S., Barka, A.A., Dieterich, J.H., 1997. Progressive failure on the North Anatolian fault since 1939 by earthquake stress triggering. Geophys. J. Int. 128, 594–604.
Tapponnier, P., Molnar, P., 1977. Active faulting and tectonics in China. J. Geophys. Res. 82, 2905–2930.
Tapponnier, P., Xu, Z., Roger, F., Meyer, B., Arnaud, N., Wittlinger, G., Yang, J., 2001. Oblique stepwise rise and growth of the Tibet Plateau. Science 294, 1671–1678.
Toda, S., Stein, R.S., 2002. Response of the San Andreas fault to the 1983 Coalinga–Nuñez earthquakes: an application of interaction-based probabilities for Parkfield. J. Geophys. Res. 107 (B6), 2126. http://dx.doi.org/10.1029/2001JB000172.
Toda, S., Stein, R.S., 2003. Toggling of seismicity by the 1997 Kagoshima earthquake couplet: a demonstration of time-dependent stress transfer. J. Geophys. Res. 108 (B12), 2567. http://dx.doi.org/10.1029/2003JB002527.
Toda, S., Stein, R.S., Reasenberg, P.A., Dieterich, J.H., 1998. Stress transferred by the $M_w = 6.5$ Kobe, Japan, shock: effect on aftershocks and future earthquake probabilities. J. Geophys. Res. 103, 24543–24565.
Toda, S., Stein, R.S., Sagiya, T., 2002. Evidence from the a.d. 2000 Izu Islands earthquake swarm that stressing rates governs seismicity. Nature 2002 (419), 58–61.
Toda, S., Lin, J., Meghraoui, M., Stein, R.S., 2008. 12 May 2008 M = 7.9 Wenchuan, China, earthquake calculated to increase failure stress and seismicity rate on three major fault systems. Geophs. Res. Lett. 35. http://dx.doi.org/10.1029/2008GL034903 (L17305).
Van der Woerd, J., Ryerson, F.J., Tapponnier, P., Meriaux, A.S., Gaudemer, Y., Meyer, B., Finkel, R., Caffee, M., Zhao, G., Xu, Z., 2000. Uniform slip-rate along the Kunlun fault: implications for seismic behaviour and large-scale tectonics. Geophys. Res. Lett. 27, 2353–2356.
Van der Woerd, J., Xu, X.W., Li, H.B., Tapponnier, P., Meyer, B., Ryerson, F.J., Meriaux, A.S., Xu, Z.Q., 2001. Rapid active thrusting along the northwestern range front of the Tanghe Nan Shan (western Gansu, China). J. Geophys. Res. 106 (B12), 30475–30504.
Van Der Woerd, J., Meriaux, A.S., Klinger, Y., Ryerson, F.J., Gaudemer, Y., Tapponnier, P., 2002. The 14 November 2001, Mw = 7.8 Kokoxili earthquake in northern Tibet (Qinghai Province, China). Seismol. Res. Lett. 73, 125–135.
Van Der Woerd, J., Klinger, Y., Tapponnier, P., Xu, X., Chen, W., Ma, W., King, G., 2003. Coseismic offsets and style of surface ruptures of the 14 November 2001 Mw = 7.8 Kokoxili earthquake (northern Tibet). Geophys. Res. Abstr. (CD-ROM 5, Abstract 11151).
Wang, R., Lorenzo-Martín, F., Roth, F., 2006. PSGRN/PSCMP—a new code for calculating co- and post-seismic deformation, geoid and gravity changes based on the viscoelastic-gravitational dislocation theory. Comput. Geosci. 32, 527–541.
Wen, Y.Y., Ma, K.F., Song, T.R.A., Mooney, W.D., 2009. Validation of the rupture properties of the 2001 Kunlun, China ($M_s = 8.1$), earthquake from seismological and geological observations. Geophys. J. Int. 177, 555–570.
Wen, Y., Li, Z., Xu, C., Ryder, I., Bürgmann, R., 2012. Postseismic motion after the 2001 Mw 7.8 Kokoxili earthquake in Tibet observed by InSAR time series. J. geophys. Res. 117 (B8). http://dx.doi.org/10.1029/2011JB009043 B08405.
Xiong, X., Shan, B., Zheng, Y., Wang, R.J., 2010. Stress transfer and its implication for earthquake hazard on the Kunlun Fault. Tibet Tectonophysics 482 (1–4), 216–225.
Xu, X., 2000. Scientific survey for the Manyi earthquake. In: Liu, Y.C. (Ed.), China Earthquake Yearbook. Seismological Press, Beijing, pp. 327–329 (in Chinese).
Xu, Z.H., Wang, S.Y., Gao, A.J., 2000. Present-day tectonic movement in the northeastern margin of the Qinghai–Xizang (Tibetan) plateau as revealed by earthquake activity. Acta Seismol. Sin. 13, 507–515.
Xu, X., Chen, W., Ma, W., Yu, G., Chen, G., 2002. Surface rupture of the Kunlunshan Earthquake (M_s 8.1), northern Tibetan Plateau, China. Seismol. Res. Lett. 73, 884–892.
Zeng, Y., 2001. Viscoelastic stress-triggering of the 1999 Hector Mine earthquake by the 1992 Landers earthquake. Geophys. Res. Lett. 28, 3007–3010. http://dx.doi.org/10.1029/2000GL012806.
Zhang, C., Shi, Y., Ma, L., Lomnitz, C., 2007. A rheological model of post-seismic deformation for the 2001 Kunlun, China earthquake, Mw 7.8. Geofiz. Int. 46 (3), 145–154.